Surveys in Geophysics (2005) 26: 307–339
DOI 10.1007/s10712-005-1885-1

OBSERVATIONS OF A UNIQUE CUSP SIGNATURE AT LOW AND MID ALTITUDES

W. R. KEITH[1,2], J. D. WINNINGHAM[1], M. L. GOLDSTEIN[2], M. WILBER[3], A. N. FAZAKERLEY[4], H. RÈME[5], T. A. FRITZ[6], A. BALOGH[7], N. CORNILLEAU-WEHRLIN[8] and M. MAKSIMOVIC[9]

[1]*Southwest Research Institute, P. O. Drawer 28510, San Antonio, TX 78228-0510, USA*
E-mail: wayne.keith@gsfc.nasa.gov;
[2]*NASA Goddard Space Flight Center, Code 612.2, Greenbelt, MD 20771, USA;*
[3]*University of California, Space Science Laboratory 7450, Berkeley, CA 94720, USA;*
[4]*Mullard Space Science Laboratory, Holmbury St Mary, Dorking, Surrey RH5 6NT, UK;*
[5]*CESR, BP 4346, 9 Ave Colonel Roche, Cedex, Toulouse 31029, France;*
[6]*Boston University, Center for Space Physics, 725 Commonwealth Ave, Boston, MA 02215, USA;*
[7]*Imperial College Space and Atmospheric Physics group, The Blackett Laboratory, London, UK;*
[8]*CETP, 10-12 Ave de Europe, Velizy, 78140, France;*
[9]*LESIA and CNRS, Paris Observatory, 61 Ave de l'Observatoire, France*

(Received 20 January 2003; Accepted 30 April 2004)

Abstract. Observations of a unique cusp feature at low and mid altitudes are reported. This feature has a consistent double-peaked or "V"-shaped structure at the equatorward edge of high-latitude particle precipitation flux, and is predominantly present for high IMF B_y conditions. The observations are consistent with the Crooker ('A split separator line merging model of the dayside magnetopause', *J. Geophys. Res.* 90 (1985) 12104, 'Mapping the merging potential from the magnetopause to the ionosphere through the dayside cusp', *J. Geophys. Res.* (1988) 93 7338.) antiparallel merging model, which predicts a narrow wedge-shaped cusp whose geometry depends greatly on the dawn/dusk component of the IMF. Various observations are presented at low altitudes (DE-2, Astrid-2, Munin, UARS, DMSP) and at mid altitudes (DE-1, Cluster) that suggest a highly coherent cusp feature that is consistent with the narrow, wedge-shaped cusp of Crooker (1988), and contains persistent wave signatures that are compatible with previously reported high-altitude measurements. A statistical survey of Astrid-2 and DMSP satellite data is also presented, which shows this feature to be persistent and dependent on the IMF angle at the magnetopause, as expected. Thus, the cusp signatures observed at a wide range of altitudes present a coherent picture that may be interpreted in terms of a footprint of the magnetopause current layer.

Keywords: cusp, true cusp, magnetosphere

Abbreviations: ISEE: International Sun–Earth Explorers; GSE: Geocentric Solar Ecliptic; GSM: Geocentric Solar Magnetic; ACE: Advanced Composition Explorer; CODIF: Composition and Distribution Function Analyzer; DMSP: Defense Meteorological Satellite

Program; FFT: Fast Fourier Transform; ESA: European Space Agency; HIA: Hot Ion Analyzer; MHD: Magnetohydrodynamics; UT: Universal Time; RAPID: Research with Adaptive Particle Imaging Detectors; VEFI: Vector Electric Field Instrument; SSJ: Special Sensor Aurora Particle; STAFF: Spatio-Temporal Analysis of Field Fluctuations; DE: Dynamics Explorer; HEPS: High-Energy Particle Spectrometer; MEPS: Medium-Energy Particle Spectrometer

1. Introduction

Ever since Chapman and Ferraro (1931) first induced the basic nature of the Earth's magnetosphere, its 2-D and 3-D topology has indicated the existence of a dayside magnetic cusp. In the past, however, understanding the geometry and dynamics of the cusps has been limited by the simple 2-D cut planes used to describe them. The term "cusp" itself demonstrates the historical bias towards 2-D representations, since only in a 2-D cut plane does this region fit the mathematical definition of a point of reversal on a curve. This cusp, or weak magnetic field region, is invariably near magnetic local noon at the latitude where magnetic field lines switch from closing on the dayside to being mapped back into the tail. This geometry was thought to allow for more or less direct penetration of magnetosheath particle fluxes to low altitudes. Early observations (Heikkila and Winningham, 1971) showed a high-latitude band of low-energy particle precipitation with magnetosheath-like properties on the dayside at low altitudes. They interpreted this feature as the long sought for evidence of direct solar wind entry via a magnetic cusp. This general region of particle penetration was later separated into a "cusp proper" and a "Cleft/Boundary Layer", representing separate particle entry processes (i.e., direct and indirect) (Newell and Meng, 1988). This terminology builds upon the "cusp" versus "cleft" distinction of Heikkila (1972) and Reiff (1979), who argued that the "cusp" represented direct entry whereas the "cleft" was the low-altitude signature of the Low Latitude Boundary Layer.

Newell and Meng (1988) defined the low-altitude cusp proper as the subregion of plasma flux that more closely resembles magnetosheath plasma spectral characteristics, indicating "more direct" entry than that associated with low altitude access via the Low Latitude Boundary Layer (LLBL), the plasma region just equatorward of the cusp representing plasma near the magnetopause but inside the magnetosphere. This definition results in a cusp of much narrower extent in Magnetic Local Time (MLT) and Invariant Latitude (IL), and is limited to fairly direct plasma entry processes (i.e., little or no acceleration of the magnetosheath population). This smaller, more directly connected region is continuously present with a density that remains consistent with solar wind density variations (Aparicio et al., 1991).

The cusp proper averages approximately 2 to 3 h in longitude centered at noon, and about 1° to 5° in IL centered at about 78° IL (1° $\approx$ 100 km at

100 km altitude) (Newell and Meng, 1988; Lundin 1998; Aparicio et al., 1991). Its location and size vary with changes in the IMF direction and solar wind dynamic pressure, but it is always present (Newell and Meng, 1988). The above size and location represent statistical averages and are quite large. At low altitude (< 1000 km polar circular orbit), a feature of this size will be traversed on average in about 15 s to a minute. Trajectories not cutting through the center of the cusp would have even shorter traversal times, on the order of a few seconds. Orbits with more equatorward inclinations may spend more time in the cusp, depending on how much local time is covered while inside the appropriate latitude range. A theoretical maximum for a cusp traversal (3 h of local time at about 77° latitude) would be on the order of 8 min. It is important to note that while the quick traversals of the cusp at low altitude may have limited the detail seen in the past, they have the advantage of being more of a "snapshot", with the data less likely to be contaminated with temporal changes during the traversal. The faster sample times of recent instruments (described in the Appendix A) allows the detail to be seen without the need to rely on higher altitudes and slower traversals, with the concomitant intermixing of populations due to horizontal transport. That is, mid-altitude measurements, while showing many similar particle characteristics, may contain bounced and tailward convected populations that may have histories different from the downcoming particles.

Extending the concept of antiparallel merging (Crooker, 1985) to the low altitude cusp, Crooker (1988) proposed a mapping of the potential drop along the merging line at the magnetopause down to the ionosphere via the cusps. The antiparallel model predicts a stretched cusp radiating away from the classical cusp point (i.e., where the cusp would be without interconnection of the fields), with the potential drop across an increasingly shorter distance along the magnetopause mapping to points further from this classical location. In order to maintain a realistic distance across which this potential is applied, the cusp must be wedge-shaped, with its base at the classical cusp point and the full potential drop applied across it (Figure 1). The edges of the wedge would map to the innermost regions of the magnetopause along the neutral line, moving to the outer surface as one moves towards the center of the wedge (Stasiewicz, 1991).

Another result of this topology of interconnected field lines is that this distended cusp rotates about its base with variations in the y-z plane (in GSM coordinates) of the Interplanetary Magnetic Field (Figure 2). For a purely southward IMF the wedge is wide with the point facing towards lower latitudes, and resembles the more generally conceived large ovoid cusp. As B_y increases, though, the tip begins to swing in the direction of the B_y component, until for a purely B_y case the point of the wedge faces duskwards perpendicular to its southward orientation. As B_z becomes more positive, this cusp wedge continues to rotate and become thinner (since the total potential

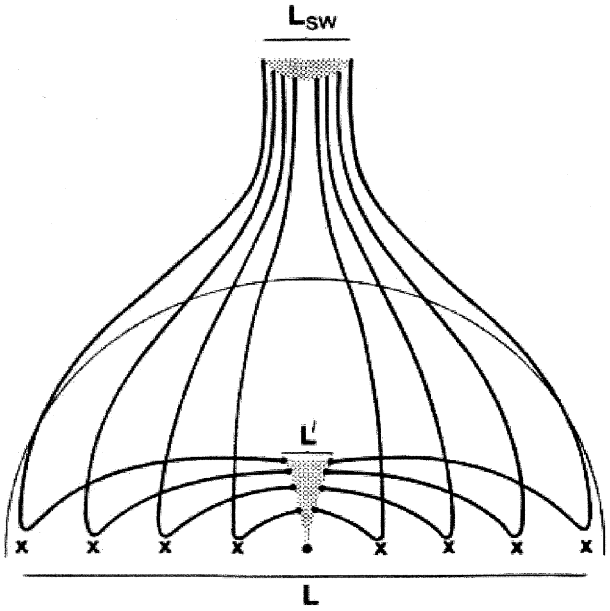

Figure 1. View from the Sun towards the Earth of southward Interplanetary Magnetic Field lines mapping the solar wind potential drop through the magnetopause down to the cusp. X's represent the places where the field lines cross the X-line. The geomagnetic (curved) field lines are shown near the magnetopause surface until they turn Earthward towards the cusp (shaded). The footprint of these 'first open' field lines thus is a wedge in the ionosphere. (Adapted from Crooker, 1988).

drop across it becomes less), until it becomes a very narrow poleward directed wedge for a pure positive IMF B_z. This type of narrow, IMF-dependent cusp wedge is consistent with the observations in the next section, in which a double-sided or "V" energy dispersion signature is seen for high IMF B_y cusp crossings. The simple three-dimensional image of the cusp as a "funnel" thus becomes a much more complex structure, depending on B_y and B_z in shape as well as location. A single satellite track can encounter very complex spatial structures in the cusp, although until recently it has been very difficult to distinguish them from temporal features. The ESA/NASA Cluster multi-satellite mission has begun to clarify such long-standing ambiguities.

Recent studies of the high-altitude, exterior cusp region have shown there to be a highly turbulent layer (labeled Turbulent Boundary Layer in Figure 3) containing large amplitude, low frequency waves. Savin et al. (1998) and Dubinin et al. (2002) have shown this region to be a permanent feature. Using Interball and Prognoz data, the following features of the exterior cusp shown in Figure 3 have been defined. The stagnation region (previously defined by Paschmann et al. (1976)) is broken down into the Turbulent Boundary Layer outside the magnetopause, and the Outer Cusp inside the magnetopause. The magnetopause boundary is defined as the

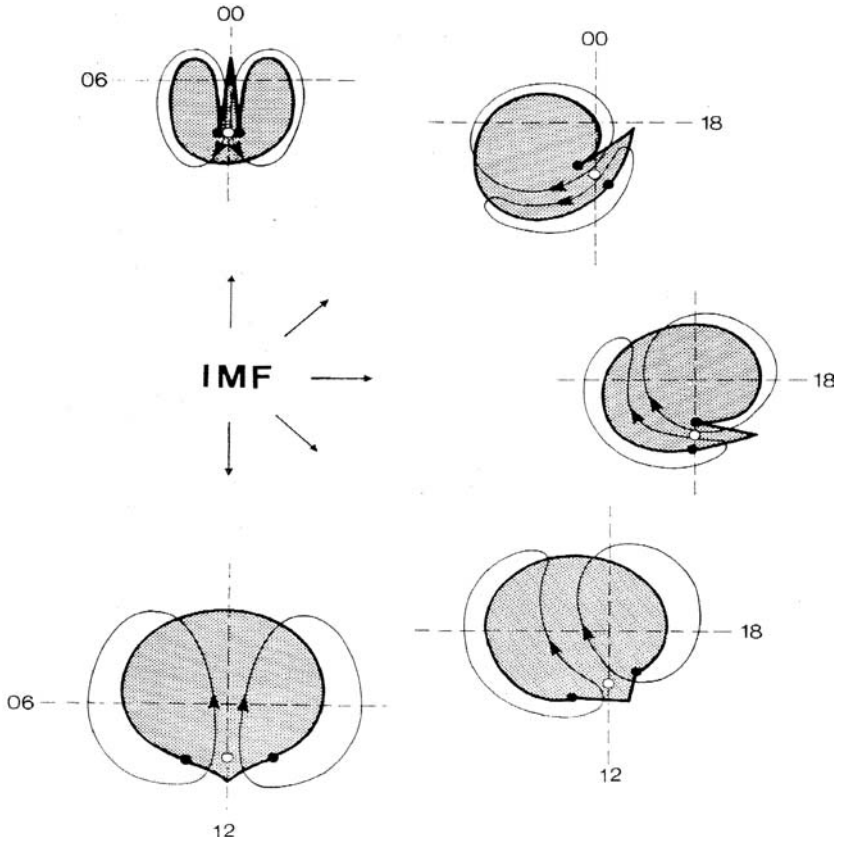

Figure 2. Schematic of the relationship between IMF angle and northern polar cap convection and cusp geometry. The Sun is towards the bottom and the view is from above the North pole. The 'wedge cusp' (where the lighter flow lines cross the heavier polar cap boundary) can be seen to narrow and rotate with changes in the IMF direction from southward (bottom) to duskward (middle) and finally northward (top). (From Crooker, 1988).

separatrix between the geomagnetic field and the IMF. The boundary is shown dashed in the exterior cusp region since the dynamic properties of the cusp often prevent an unambiguous determination of the magnetopause location. The Inner Cusp extends below these regions to low altitudes. Since the magnetopause boundary passing through this stagnation region can frequently not be identified, the distinction between the boundaries and characteristics of the sub-regions in Figure 3 may become blurred. This empirical exterior cusp model is based primarily on data from spacecraft heading outwards from the tail lobe of the magnetosphere, through the cusp, and out into the magnetosheath. Thus the extent and structure of this model in mid-altitude regions is not well defined. Multi-spacecraft mid-altitude cusp passages are now starting to facilitate refining the lower end of this exterior cusp model and its 3D, dynamic geometry.

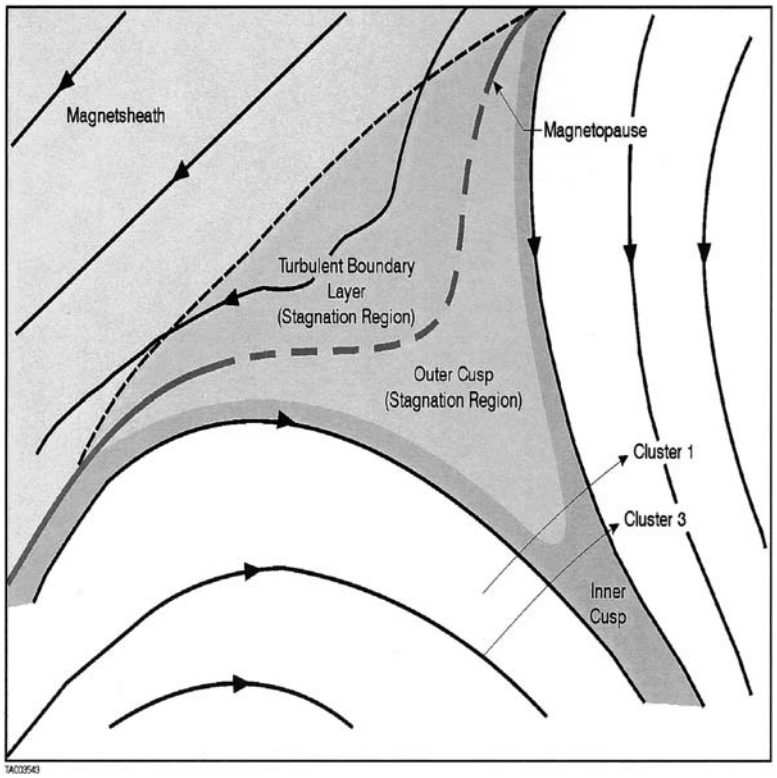

Figure 3. The regions of the exterior cusp as proposed by Savin, including external and internal field geometry. Two Cluster spacecraft trajectories are also shown (see Observations section). (Adapted from Savin et al., 1998).

2. Observations

We present data from several satellites, all of which show similar cusp signatures. Due to the large number of individual measurements involved with the observations, details of the instrumentation used are not given here. A brief description of the instruments used can be found in the Appendix A. In this section examples of data from the various satellites will be presented in order to establish the characteristics of this new signature, and to demonstrate its independence of any particular instrument, measurement or altitude. These examples are representative of the larger set of cusp passes surveyed.

2.1. DE DATA

The first example of this cusp feature comes from a pass of the DE-2 satellite on September 6, 1982 (Figure 4). LAPI particle spectrograms are from the

electron sensor with a look angle of 19° from the magnetic field (top panel) and from the ion sensor with a look direction 64° from the magnetic field. The data were taken on a southern hemisphere equatorward pass, the cusp being located at an IL of −63° and a pre-noon MLT of 10:13. A clear dispersion signature can be seen in the ion data (Figure 4, second panel), moving from lower (poleward) energies to higher (equatorward) energies,

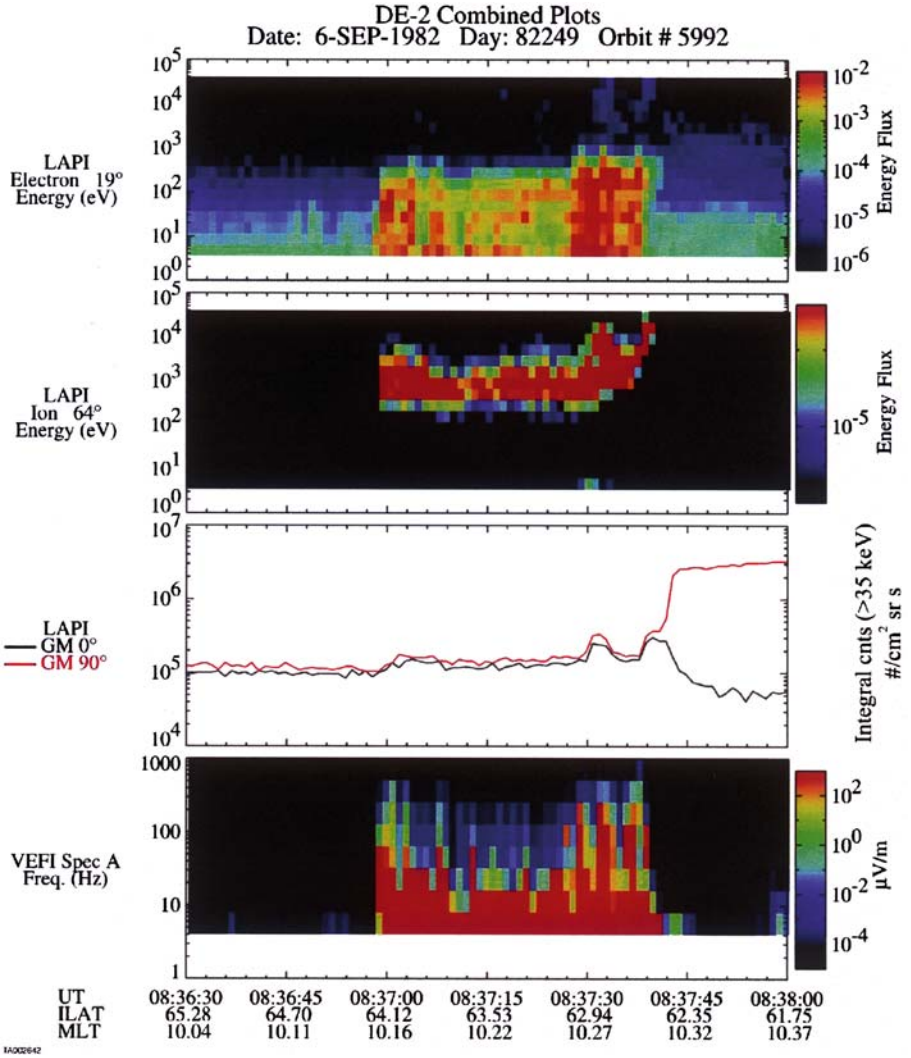

Figure 4. DE-2 data from September 6, 1982. Data were taken during an equatorward cusp pass in the southern hemisphere. The top spectrogram is for electrons measured at a 19° pitch angle. The second is for ions measured at a pitch angle of 64°. The third plot shows high energy electrons integrated for energies greater than 35 keV and 0° and 90° pitch angle, and the bottom spectrogram presents the measured square root of the electric wave power.

although the spectrogram appears to be flat at about 1 keV from 8:37:00 to 8:37:30 (all times given in UT). The feature of interest, however, is the higher-energy piece at the right-hand end of the ion spectrogram. This "V" shaped signature can be clearly seen beginning at the equatorward edge from 8:37:30 to 8:37:40. This example is at unusually high energies, with peaks at around 20 keV down to 2 keV at the center. The feature is consistent with the narrow wedge cusp of the Crooker model, with the highest energies being found towards the outer edges. The electrons (Figure 4, top panel) clearly show enhancement during this same time period, from 30 keV down to the lowest energies. Above 1 keV the fluxes vary spatially the same as the G-M data in panel 3. Below 1 keV there is a different morphology, though, remaining steady throughout the feature. The third panel of Figure 4 is Geiger–Mueller data and the parallel (black) and perpendicular (red) lines both indicate clear enhancements over their already elevated levels at the two edges of the feature and are colocated with the ion V edges. At the equatorward edge the 90° pitch angle G–M data jump to much higher fluxes, indicating trapped particles on closed field lines.

The bottom panel of Figure 4 is the square root of AC electric wave power from the VEFI instrument displayed from 4 to 1000 Hz. This spectrogram shows strong waves at 400 Hz and lower during the V. This is consistent with the turbulence seen at the magnetopause (Gurnett, 1979) and exterior cusp regions, indicating that these field lines may be connected with those regions while passing through the ion V cusp feature. The V covers about 0.4° in IL and about 18 min of MLT, which corresponds to a very narrow feature of approximately 76 km. For purposes of inter-comparison, we will also give an approximate size when projected down to 100 km. In this case, the projected width in this dimension is approximately 69 km. Examples of this type of feature are by no means unique, but can be hard to spot due to their small size, and the fact that they are very localized in IL and MLT, being found within about an hour of noon in MLT (depending on the IMF) at cusp latitudes. The ISEE 1 and 2 satellites measured the IMF during this time period to be steady and primarily duskward, with significant southward and tailward (B_x) components. Duskward IMF is consistent with a pre-noon located cusp in the southern hemisphere. Strong B_y and weakly southward IMF is also consistent with a passage across a narrow wedge cusp as described above.

The DE-1 spacecraft traversed the mid-altitude cusp on October 1, 1981 (Figure 5). In this case the particle data were recorded by HAPI. This is an example of a mid-altitude crossing of the cusp, about 18,850 km in altitude (3.96 R_E geocentric distance). The top spectrogram is of electrons, and the second ions, both measured in the spin plane of the satellite. The line overplot on the top panel shows the flux of electrons integrated between 2 and 25 keV, and highlights the morphology of the higher-energy electrons. The third and

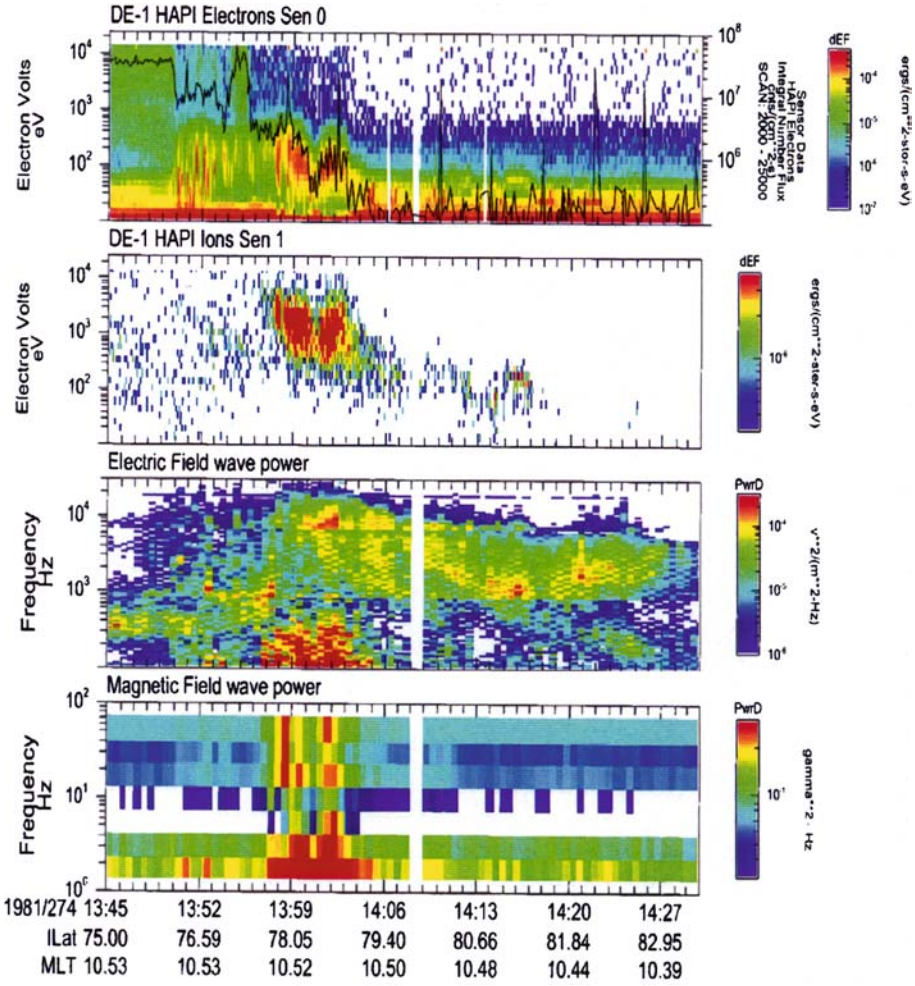

Figure 5. DE-1 data from October 1, 1981. Data were taken during an equatorward cusp pass in the northern hemisphere. The top two spectrograms are for electrons and ions measured in the spin plane. The third and fourth give electric and magnetic field wave power.

fourth panels are proportional to the electric and magnetic wave power, respectively. The data were taken in the pre-noon sector, on a poleward pass in the northern hemisphere. The feature is seen in the ions (second panel) beginning at 13:59 at about 2 keV. The ion flux decreases in energy and intensity to about 500 eV a minute and a half later, only to return to the original values at 14:03. This morphology is typical and very much like the lower-altitude pass described. The electron intensities peak as well during the time of the ion V, with the highest energy particles showing the transition from closed to open field lines. The electric and magnetic field wave power shown in the bottom two spectrograms show a typical increase, especially at

the lowest frequencies, during the passage through the feature. The width of the satellite track through this cusp sub-region is about 1125 km, which translates to a 100 km footprint of about 148 km. This is very consistent with the size range seen at other altitudes. The IMF during this time was strongly positive in B_x, with equally weaker positive B_y and negative B_z.

2.2. DMSP DATA

Particle data from the SSJ/4 instrument of the DMSP-F10 satellite can be seen in Figure 6. The data presented are from March 28, 1992, when the satellite was passing equatorward over the cusp at an IL of 73° and a MLT just post noon (12:20). The ion data (lower panel) again exhibit the energy-latitude dispersion as it passes from higher to lower latitudes, and also clearly show a "V" structure beginning at 10:10:55 UT which lasted just under 25 s. The peak energy of the poleward edge of the structure is slightly less in this case, about 1 keV; however, the middle and equatorward edge are peaked at

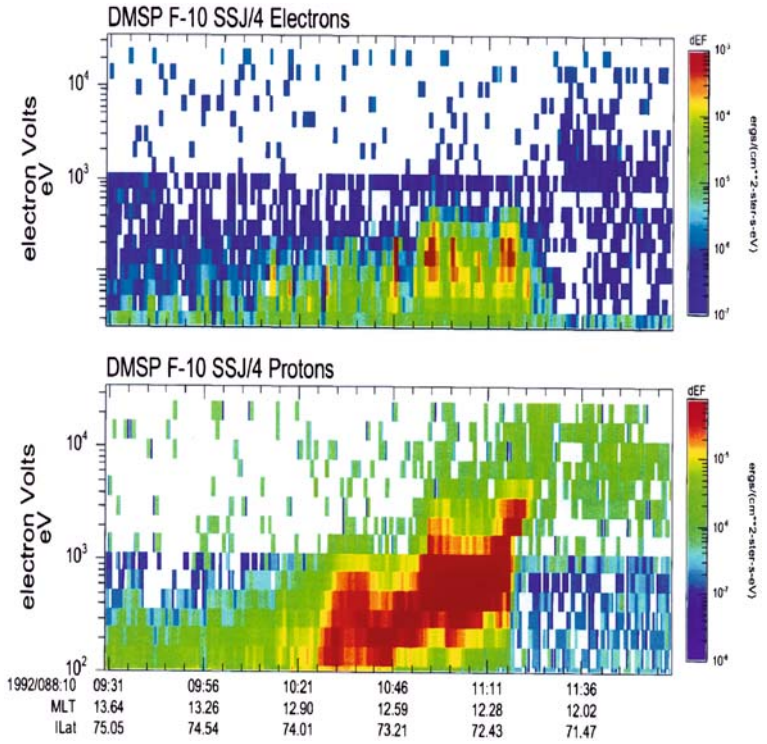

Figure 6. DMSP F-10 data from March 28, 1992. Data were taken during an equatorward cusp pass in the northern hemisphere. The upper spectrogram is for electrons, and the lower spectrogram ions.

500 eV and 2 keV, respectively. This is typical for many of the examples we have studied. The corresponding electron (upper panel) enhancements at the edges are also typical, being mostly in the 100 to 200 eV range. The satellite altitude at the time of the pass was 770 km, and the feature spanned 0.77° of Invariant Latitude, giving it a latitudinal width of about 96 km (84 km at 100 km) and an orbital track of just over 178 km (156 km at 100 km). As for other cases this is very small, on the order of a proton gyroradius at the magnetopause. IMF data for this time period are not available.

A second DMSP-F10 passage can be seen in Figure 7. The plot format is the same as in the previous example. These data were taken on September 25, 1991, during another equatorward northern cusp pass. The IL is 70.5° at a pre-noon MLT (11:20) at the time of the V signature in the ion data from 8:15:40 to 8:16:10. This pass is fairly typical, except that the low energy tail poleward of the feature of interest is slightly separated. This may represent a temporal change, or a particularly unusual crossing geometry. The crossing geometry is probably also the reason why the poleward edge of the V appears to be compressed and has a lower peak energy than the equatorward side,

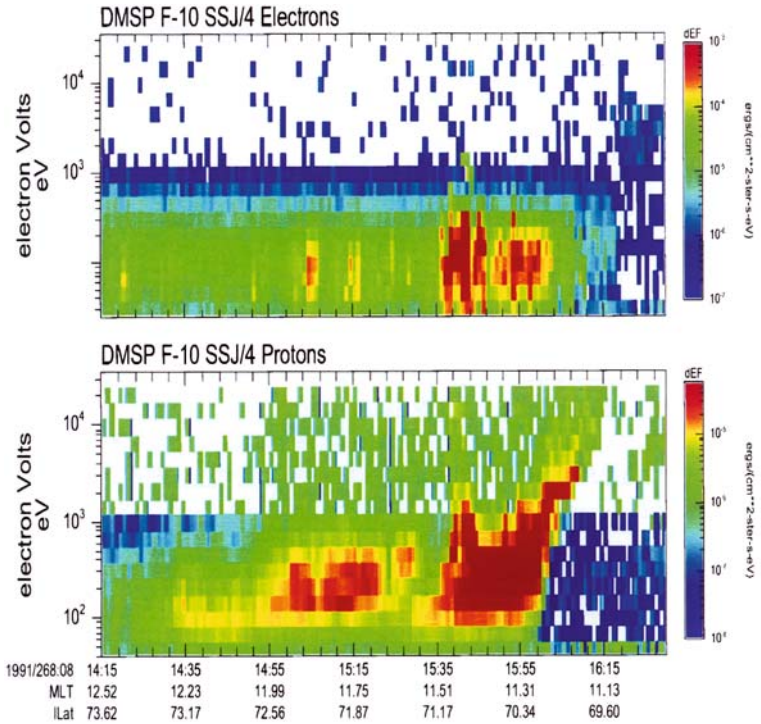

Figure 7. DMSP F-10 data from September 25, 1991. Data were taken during an equatorward cusp pass in the northern hemisphere. Upper spectrogram is for electrons, and the lower spectrogram ions.

giving a lopsided or "J" shaped appearance to the feature. This is similar to the other DMSP example shown in Figure 6. The total size of this feature is slightly larger, though, covering 1° of Invariant Latitude at an altitude of 815 km. This equates to a latitudinal width of 125 km (108 km at 100 km) with an orbital track distance of 213 km (185 km at 100 km), similar to the other cases. The IMF at this time was over 10 nT in B_y and almost −5 nT in B_z.

2.3. Astrid-2 data

Data from the MEDUSA and EMMA instruments aboard Astrid-2 are shown in Figure 8. The data were taken on January 13, 1999, during a pass over the southern auroral zone. The spacecraft was traveling equatorward at an altitude of 1029 km. In the antiparallel (downward moving) ion spectrogram (Figure 8, bottom panel), a typical dispersion signature can be seen, with a long section that is nearly flat at about 300 eV from 20:12:49 to 20:13:13. The region of interest, however, is less than a third of this dispersion pattern, at the equatorward edge from 20:13:16.5 to 20:13:28. It stands out as a sudden increase of about 1.5 keV (from 500 eV to 2 keV) in the peak energy of the ions. The peak energy of the feature then dips to about 1 keV at 20:13:21.5 and becomes weaker in intensity. From this point until 20:13:28 the energy steadily increases back to 2 keV. This 10-second interval clearly has the V shaped ion structure, with higher energies on the edges and lower energies towards the center. Many of the older-style instruments discussed in this paper have sweep resolutions of 1 to 8 s, which would hardly be enough to identify this feature. MEDUSA, however, has an ion sweep resolution of 0.125 s, so it can easily distinguish this crossing. The ions cut off abruptly on the equatorward edge of the cusp at 20:13:30. The same feature is present in the mirroring perpendicular pitch-angle ions, and the 2 keV "wings" appear in the parallel (upwards) ions, however, the lower energy central portion is not present. In these latter two spectrograms (Figure 8, second and third from the bottom), low-energy enhancements (3–100 eV) can also be seen at the beginning (20:13:18) and end (20:13:25) of the feature moving up the field line. The middle three spectrograms contain the medium energy electron data. The antiparallel (downwards) electrons (sixth panel from the top) and to a lesser extent the other pitch-angle electrons, also show < 300 eV enhancements at 20:13:18 and 20:13:25.

EMMA electric and magnetic field data are shown in the fourth through seventh panels of Figure 8 (line plots). For the data presented here, the electric field along the direction of the magnetic field has been assumed to be zero, and the two perpendicular components in the eastward and equatorward directions have been calculated. (This assumption is consistent with other low-altitude spacecraft results (Bonnell et al., 1999).) The magnetic field

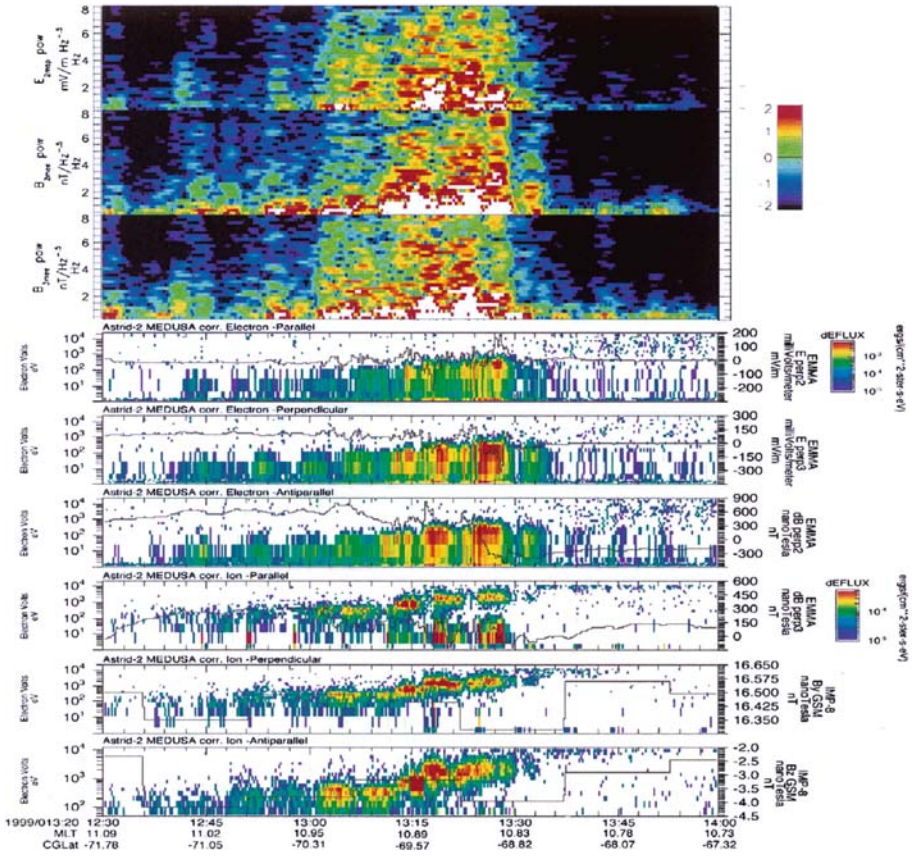

Figure 8. Astrid-2 data from January 13, 1999. The data were taken during an equatorward pass through the southern cusp region. The top three panels contain frequency–time spectrograms of electric (top) and magnetic (second two) waves up to 8 Hz. The middle three panels show electron fluxes and the bottom three panels ion fluxes. For both the electrons and ions, the top panel is for particles at 'zero' pitch angle (flowing up the field line), the middle for trapped particles (90° pitch angle) and the bottom for downcoming particles (180° pitch angle). The fourth and fifth panels also contain line plots of the two perpendicular electric field components (with a scale on the right). Panels six and seven display residual magnetic field intensity (after subtracting a model field) for the same two perpendicular directions as the electric field. The bottom two line plots are the y and z components of the IMF as measured by IMP-8.

direction makes an angle of −23° with the spacecraft spin-plane at the time of this cusp crossing. Linear scales for the electric and magnetic field data are shown on the right hand side of the bottom six panels, and are in units of mV/m and nT, respectively. The electric field in the fourth (eastward) panel fluctuates about −10 mV/m outside of the cusp, but begins to gain amplitude going into the high-latitude end of the dispersion feature at about 20:13:00. The field peaks to −225 mV/m at the poleward edge of the ion feature at

20:13:16.5. After this, it increases steadily to 200 mV/m at the equatorward end of the feature (20:13:28), and afterwards settles to 0. The equatorward (North, in this case) pointing perpendicular electric field in the fifth panel begins at a potential of 100 mV/m before dropping by 250 mV/m at the poleward edge of the V. It then returns to its original value of 100 mV/m in the center before plunging to −300 mV/m at the far edge of the feature. It then settles to approximately zero as well. The electric field is V shaped about the centerline and does not reverse direction along the line of the satellite track, which is approximately in the North/South direction (i.e., the equatorward electric field always shows a negative deflection from its equilibrium value). The integrated potential is the order of 50–70 kV. This does not represent the maximum of potential difference, as the satellite does not cross the maximum contours. This is consistent with Crooker's (1988) idea of a concentrated electric field in the throat.

The detrended (delta) magnetic field data are shown on the fourth and third from the bottom panels of Figure 8 for the same two directions as the electric field data. The upper (eastward) component goes from 600 nT before the V, down to −150 nT at the end, revealing a significant current system in that one limited region. Northward data in the lower (equatorward) panel also show a net drop of about 200 nT over the feature, although the trend is much less obvious in this case. The bottom two panels contain line plots of the GSM y and z components of the Interplanetary Magnetic Field, as measured by IMP-8. These values have not been time-shifted to account for the solar wind; however, they are representative of the delayed values for this pass (weakly southward and strongly duskward). The top three panels of Figure 8 contain values proportional to the square root of the wave power for the electric (top panel) and magnetic (second and third panels) fields. The vertical axis is in Hertz, and the color bar indicates the log of the intensity. The spectrograms for the magnetic field fluctuations are calculated by an FFT from the detrended magnetometer data perpendicular to the main field in the eastward (second panel) and equatorward (third panel) directions, and shown in $nT/Hz^{0.5}$. The square root of the electric field wave power is calculated in the same manner, and is shown at the top of Figure 8 with a color bar in units of log mV/m $Hz^{-0.5}$. The sonograms show frequencies up to 8 Hz, calculated with a four second sliding window. The time period of the ion feature, from 20:13:16 to 20:13:28, coincides with a dramatic increase of over two orders of magnitude in the wave power at all displayed frequencies.

The Magnetic Local Time of the ion V event was about 10:52, and the Invariant Latitude range covered only 0.57°, from −69.54° to −68.97°. The length of the satellite track as it crossed this feature is only 86 km (69 at 100 km) (only about 10 of the old one-second sweeps), which makes this a very small feature indeed, even in terms of the cusp proper.

2.4. Munin data

MEDUSA-2 particle data from December 20, 2000 are shown in Figure 9. The electron sector closest to antiparallel to the field (i.e. particles coming down to the Earth along the field) is shown on top, while the ions from the same look angle are shown on the bottom. The satellite was near apogee at 1826 km heading poleward over the South polar region. The structure in this case begins at 21:10:44 UT at the equatorward edge of the cusp dispersion pattern with an initial peak in the ions of about 2 keV. The ion energy quickly falls after this to about 500 eV before quickly spiking back to nearly 2 keV, about 2 s after the first peak. The feature stands out as usual in the electron data, although the intensification at the edges is hard to see due to the strong electron fluxes throughout this pass. This very small feature is visible due to the relatively high sample rate of MEDUSA-2 of two complete sweeps per second for ions and 4 sweeps per second for electrons. Similar instruments with sample intervals of 1 or more seconds would not be able to resolve such a small feature. The feature took place over an Invariant Latitude range of 0.08° centered at −82.98°. The

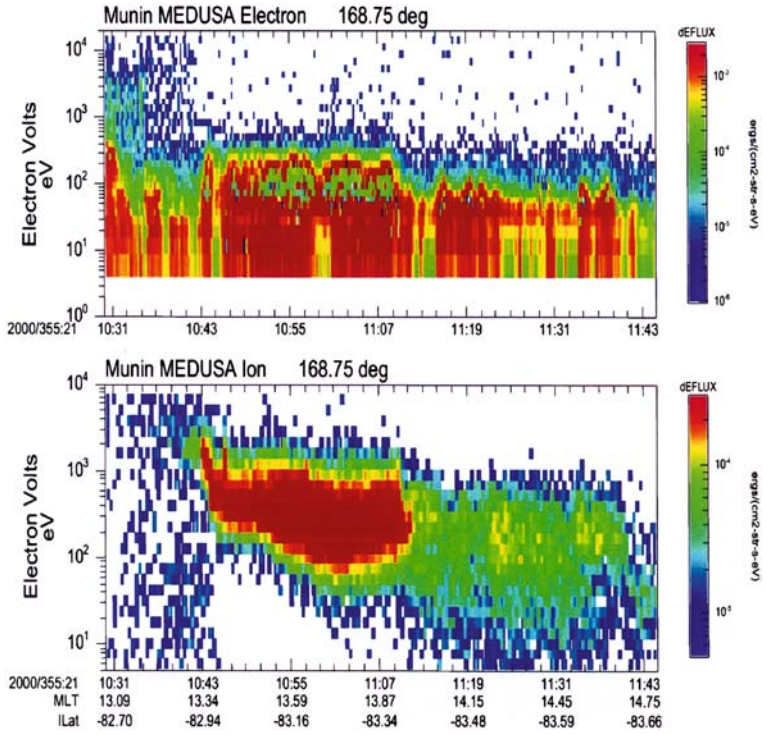

Figure 9. Munin data from December 20, 2000. Data are from a poleward cusp pass in the southern hemisphere. The upper spectrogram is for precipitating electrons, and the lower spectrogram shows the ions for the same look direction. A very small V feature can be seen at the equatorward (left) edge of the ion flux in the lower panel, near 21:10:43 UT.

Magnetic Local Time was in the afternoon sector, centered at 13:38 h. The size of the feature along the satellite track was an astonishing 12 km (8 at 100 km), by far the smallest such feature yet seen in the data. The IMF during this time, as measured by the ACE spacecraft, was weakly northward and strongly duskward. Since the cusp wedge is expected to narrow for northward IMF, this small size is consistent with theory.

2.5. UARS DATA

HEPS data presented here (Figure 10, lower two spectrograms) show electrons from one of the near-zenith pointing detectors, and protons from one of the LEP detectors. The MEPS data here (upper two spectrograms) are electrons and ions from the detector that has a look direction of 36.6° with respect to the spacecraft zenith (Winningham et al., 1993). The time resolution is 2 s for MEPS, and 4 and 8 s for HEPS electrons and protons, respectively. Data from a cusp pass are presented in Figure 10, and were taken on November 9, 1991, while UARS was heading poleward at an altitude of about 600 km. The feature of interest is located in the afternoon (13:30) sector in MLT and about −67° IL. A V-shaped feature can be distinguished which lasts about 40 s in the MEPS ion data (second panel). It begins at 05:40:40 at about 2 keV, decreases to 500 eV in the center (05:40:56) and increases back to 2 keV at 05:41:17. In contrast to many of the other examples, no ions are seen poleward of the V structure. The MEPS electron data (top panel) over this same time period show enhancements centered on about 40 eV at the beginning and end, with a strong flux of 100 eV electrons throughout the event. Notice the softening of the electrons at the ends, where the density is the highest. HEPS high-energy particle data (lower two spectrograms) also show significant enhancements at the edges of the feature at all energies up to the maximum plotted, about 300 keV. Equatorward of the feature, both electrons and ions show very large fluxes, which indicates that the particles are trapped on closed field lines. From 05:40:26 to 05:40:43, the HEPS electrons (second from the bottom) falls off steadily, corresponding to the beginning of the MEPS ion feature. There is also a significant increase in the flux of electrons at the poleward edge of the feature at 05:41:16, which peaks at or below the low-energy cutoff of 40 keV. The flux of LEP protons (bottom panel) decreases at the onset of the feature in a similar way to the HEPS electron flux, and also shows an increase at all energies at the opposite end (05:41:16).

The B_y magnetic field (line plot in third from top panel of Figure 10), which is fairly constant before and after the feature, is very disturbed during the period from 05:40:33 to 05:41:19, increasing sharply and then decreasing steadily during this time period, with a sharp rise at the end. This implies field-aligned currents directed upwards at the edges and downwards in the

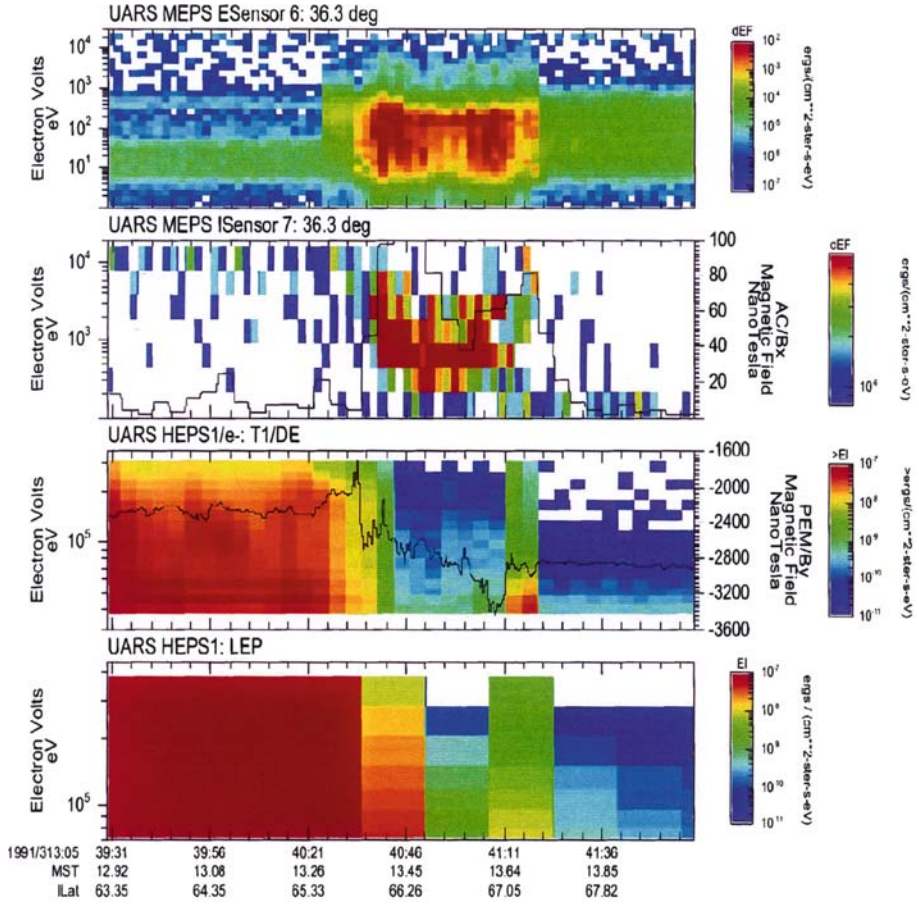

Figure 10. UARS data from November 9, 1991. The top two spectrograms are for medium energy electrons and ions, while the lower two are for high energy electrons and ions. The upper line plot is the integrated square root of magnetic wave power, while the lower line plot is magnetic field perpendicular to the spacecraft.

center. The square root of magnetic wave power data, integrated from 0 to 100 Hz and labeled AC/B_x (the scale is on the right of the second panel), increases by over an order of magnitude to 100 nT at the onset of the ion feature, dips down to about 40 nT near the center at 05:41:01, and then peaks again at 80 nT at the end of the structure before returning to low (below 10 nT) values. The invariant latitude covered during this time, though, is only 1.2°, which is about 143 km in the North/South direction, or 127 km projected to 100 km altitude. This pass, however, also had a significant East/West velocity component, which gives an orbital distance of almost 280 km (248 at 100 km), mostly in MLT. This is at the high end of sizes for this type of feature at low altitudes, a factor of 3 larger than the Astrid-2 feature, but

still at the very bottom of the range of normal cusp sizes. The IMP-8 satellite measured the IMF at this time to be weakly southward and very strongly duskward.

2.6. Cluster data

Data from August 16, 2001 mid-altitude cusp pass of the four Cluster spacecraft are shown in Figures 11–14. The data were taken during a poleward pass over the northern cusp at a geocentric distance of about 5.4 R_E (distances range for the four Cluster spacecraft in order from 5.63 R_E at Cluster-1 to 5.3 R_E at Cluster-4). The invariant latitude for all spacecraft at the cusp passage was about 78°, and the MLT was just after 14:00. This is consistent with an afternoon-shifted cusp, which is expected from the dominant IMF $+B_y$ seen by ACE at this time (with the appropriate propagation delay from ACE to Cluster).

Figure 11 shows data from all four spacecraft, two panels each; the time axis is common to all observations. RAPID >30 keV ions (black) and a detrended magnetic field (green) are shown in the upper plots, and STAFF magnetic wave power spectrograms from 8 Hz up to 4 kHz and plasma pressure derived from the PEACE electrons (red) in the lower plots. A time shift indicating when each successive spacecraft was on approximately the same given field line is indicated by the blue vertical bars. This location was set for the lead spacecraft Cluster-4 at the time that the internal magnetospheric ion flux drops off (black line in panel 7). Times when the invariant latitude and magnetic local times of the other spacecraft most closely matched those of the Cluster-4 time were subsequently marked (panels 1, 3, and 5). These marks agree remarkably well with the time that the internal source ion cuts off. The periods of enhanced wave power correspond to the periods of intensified medium energy ions and electrons shown below.

Figure 12 shows a view from the Orbit Visualization Tool (OVT) of the four satellite tracks from 9:30 to 10:30 UT as projected onto the *x*-*z* GSE plane. The actual tracks fall nearly in this plane, and are separated almost exclusively by altitude. The spacecraft markers (and associated field lines) are for the times listed next to each marker, which correspond approximately to the times of the blue vertical bars of Figure 11. The positions agree with the equatorward edge of the model cusp used in the OVT software (T87).

Figures 13 and 14 show ion and electron spectra at 0°, 90°, and 180° pitch angles for spacecraft 1 and 3, respectively. CIS/HIA (ion) data are unavailable for 2 and 4, however, the PEACE electron data (not shown) suggest that the morphology of the plasma at Cluster-2 is similar to that at 1, while the plasma at Cluster-4 is much like that at 3. The data in Figure 14 (Cluster-3) show a signature consistent with the previous low altitude cases. At the equatorward edge of the cusp, the downward (0° pitch angle) ion flux intensifies at about

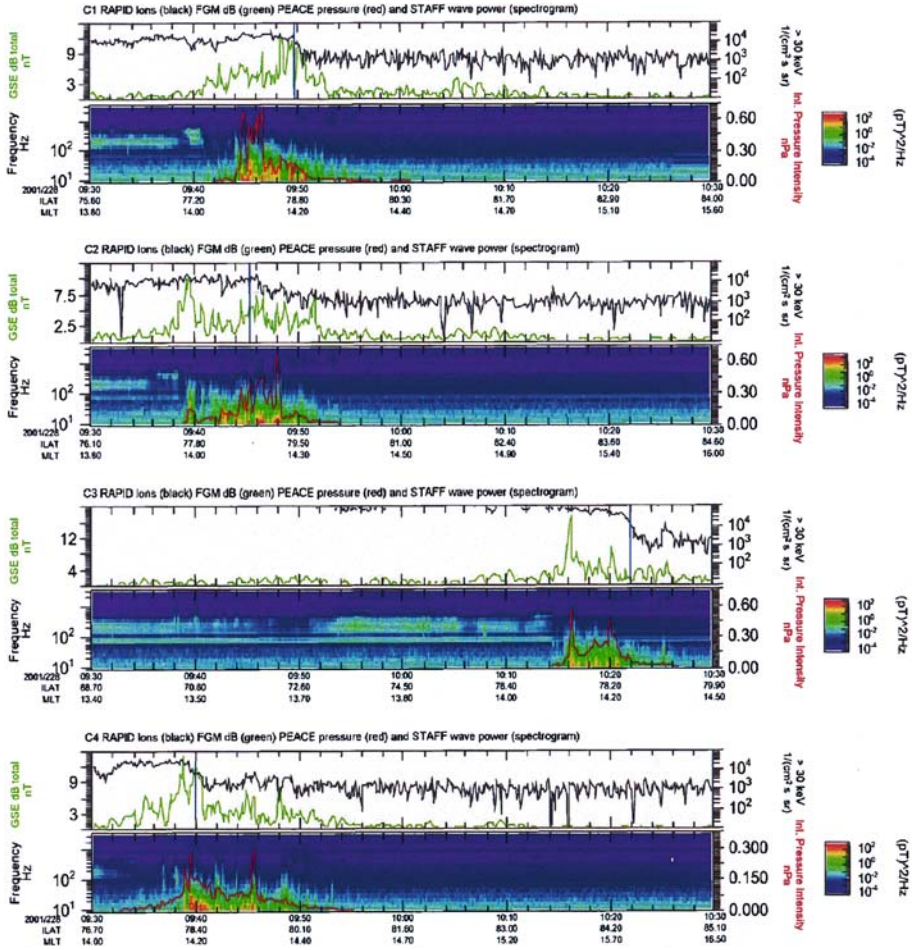

Figure 11. Cluster data from August 16, 2001. Each pair of panels corresponds to one of the four spacecraft, ordered 1 to 4 from top to bottom. Line plots on panels 1,3,5, and 7, are high energy ions (black) from RAPID and delta B (green). Spectrograms are wave power from STAFF data, while line plots over the spectrograms are electron pressure.

1 keV at 10:15:30, then drops to about 300 eV in the center at 10:17:30 before returning to over 800 eV at 10:20. The electrons also show a morphology similar to the low-altitude data, with large enhancements at the edges of the feature and elevated fluxes in between. In Figure 13 (Cluster-1), however, the dominant flow direction of the plasma changes directions many times as seen in the peak fluxes of the parallel and anti-parallel panels (first and fourth panels). These reversals are also evident in the moments data (not shown). They disrupt the cusp feature under study, although some properties such as its size and energy range remain intact. The magnetic wave properties at this spacecraft also indicate fully developed turbulence as seen in the external cusp (turbulent

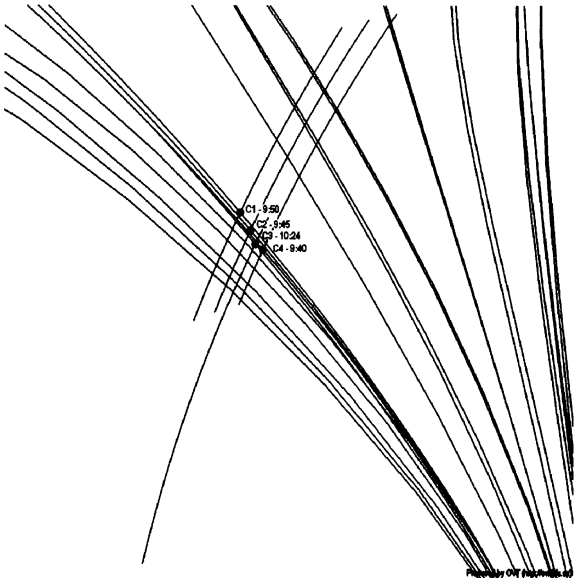

Figure 12. Cluster spacecraft satellite tracks in the GSE x–z plane from 9:30 to 10:30 UT. The Sun is to the left and the spacecraft are traveling towards the North ($+z$). The curved lines originating in the lower right corner are magnetic field lines connecting to the Earth (not shown). The spacecraft markers are displayed at the times shown for each, corresponding to their entry into the cusp field region. See Figure 3 for context. (Adapted from OVT output images).

boundary layer) region. Comparing the available data at all spacecraft and ordering by their similarities to the low-altitude V cusp crossings or the high-altitude turbulent cusp crossings, the order is the same as the spacecraft altitudes, with Cluster-4 being the most similar to low altitude data and Cluster-1 the most similar to high altitude data. Cluster-4 is also the only one to show the high-energy ion cutoff at the beginning of the feature, as the low altitude crossings show. This is despite the fact that three of the spacecraft (1, 2 and 4) traverse this feature at approximately the same time, while Cluster 3 follows about half an hour later. This would imply that the differences in the plasma characteristics are due more to the spatial separation in altitude rather than in the timing of the crossings (see satellite tracks in Figure 3). The cusp feature crossings are all of similar size, averaging about 1170 km across, which corresponds to a 100 km footprint of 98 km.

3. Statistical survey

In order to understand this unique feature in more detail, and its correlation with factors such as the interplanetary magnetic field (IMF), a statistical

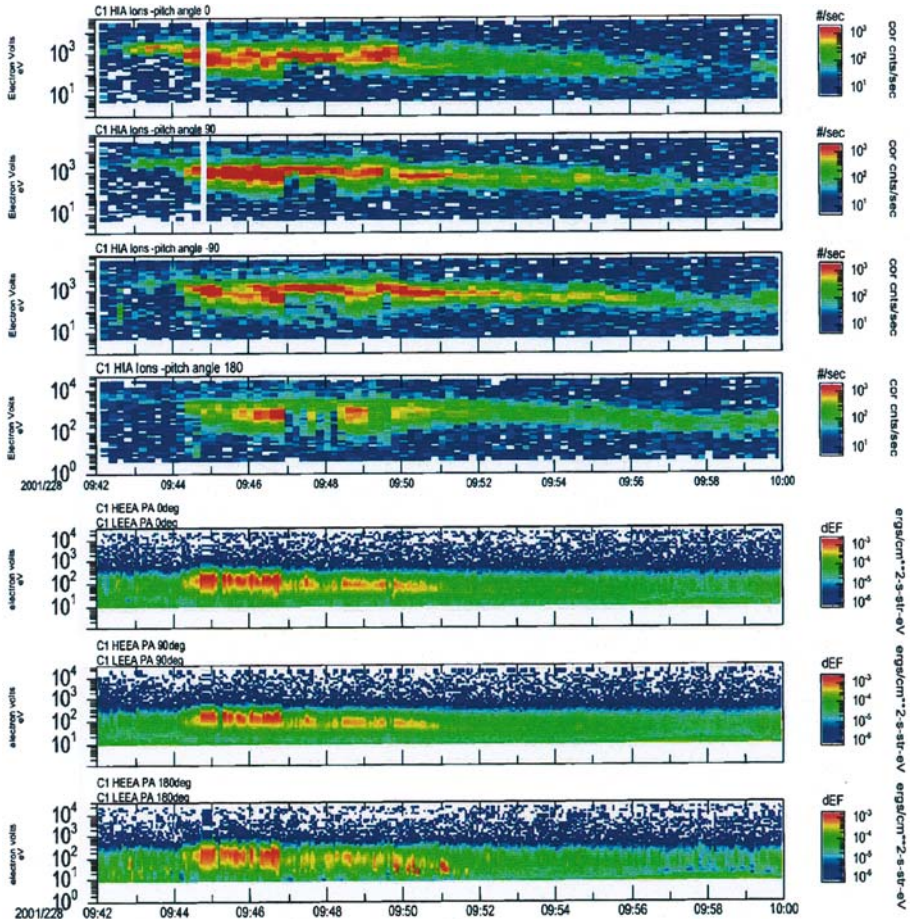

Figure 13. Cluster-1 data from August 16, 2001. The top four panels are for HIA ions in the parallel, perpendicular, and antiparallel directions. The bottom three panels are for PEACE electrons, for the same pitch angle directions.

survey was undertaken. The survey produced a set of time-tagged cusp passes for 4 of the DMSP satellites (F8, F9, F10, and F11) and Astrid-2, with the time-delayed IMF given as a clock-angle sector. This allowed a large number of passes (> 3700) to be evaluated quickly, taking into account the prevailing IMF for the pass. The primary goal of this survey is to determine the consistency of the "V" feature and to correlate it with position and IMF. Also, a rough frequency estimate may be made, keeping in mind that the feature and the satellite tracks are both very narrow, and so will not necessarily intersect even when all other conditions are favorable.

Although this study of a large number of cusp passes highlighted the almost infinite variety of particle signatures that may be encountered, for this study it was necessary to limit the scope of the survey to finding those events

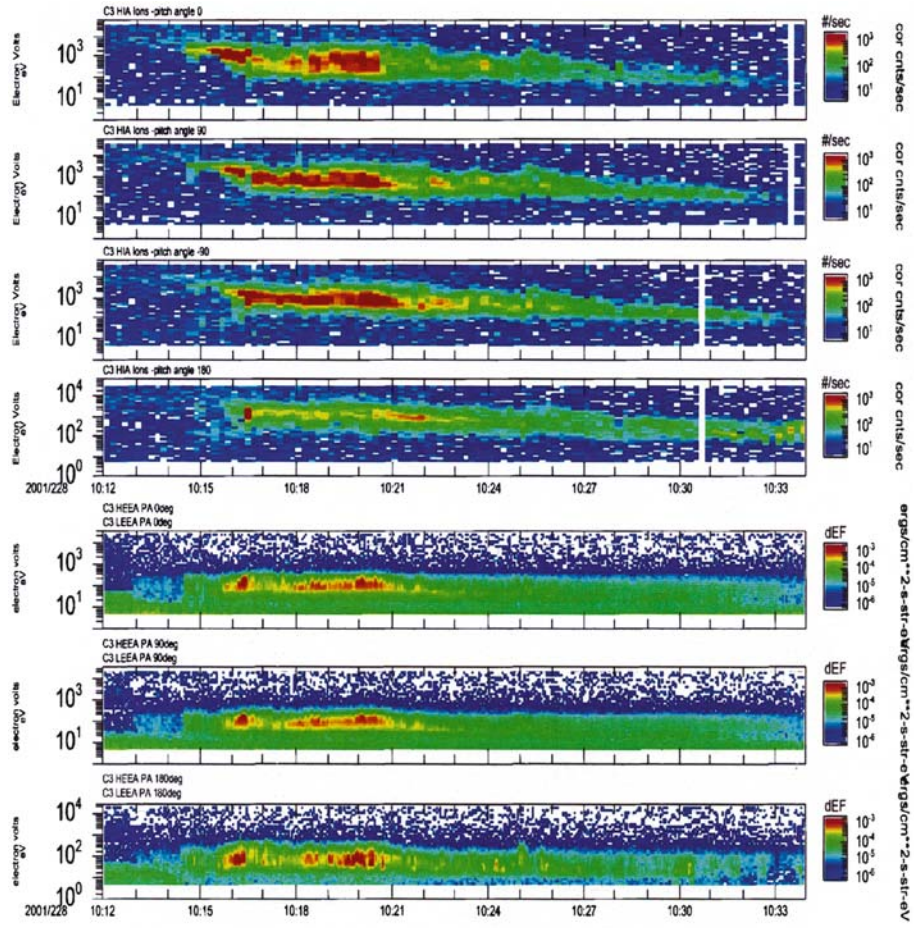

Figure 14. Cluster-3 data from August 16, 2001. The top four panels are for HIA ions in the parallel, perpendicular, and antiparallel directions. The bottom three panels are for PEACE electrons, for the same pitch angle directions.

that clearly show the defined "V" morphology. From initial observations and theoretical considerations such as the Crooker (1988) model, we expect to see these distinctive features at the equatorward end of cusp passes, and depending on the cut angle and IMF orientation, a narrow V shape in the down-going ion flux at around 1–2 keV and a scale-size on the order of 100 km. Since the size, location, and orientation of the cusp for a given set of IMF conditions is not known a priori, the relative orientation of the satellite track through the feature tends to obscure and complicate the identification for many of the passes. For example, for a given wedge cusp configuration (pure $+B_y$ in Figure 15a or pure $-B_y$ in Figure 15b) a satellite passing through the cusp may or may not cross both sides of the wedge and therefore

will not always have the expected V morphology. In both images of Figure 15, the gray satellite track would see a V, while the black satellite track would not. This orbital track bias does have an effect on the statistical analysis, as described in the Results section. The apparent continuum of V sizes in the data studied also tends to blur the distinction between the small cusp signature of interest here and larger-scale V's, which are discussed in more detail in the Discussion section. For our purposes, however, we have chosen a maximum size of 300 km for the V's, corresponding to a 40 s passage for the DMSP and Astrid-2 satellites, which have similar low-altitude circular orbits (800 and 1000 km, respectively). The majority, however, are below 100 km (about 10 s) in width.

3.1. Setup and parameters

The first step in the survey was to build a database of cusp passes for the satellites to be studied. The satellites were chosen due to the large amount of data to work from (in the case of the DMSP satellites), and their favorable orbits and instrument suites. Although the cusp is quite limited in spatial extent for a given low-altitude pass, it moves around significantly, so a fairly large "cusp box" had to be defined in the North and South directions in order to catch the majority of candidate passes. The boxes were defined as being between 10:30 and 13:30 in MLT, and the northern (southern) box at an Invariant Latitude of between 60° and 80° (−60° and −80°). The entry and

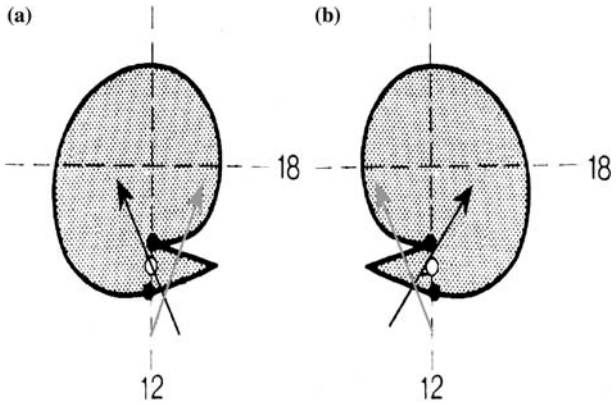

Figure 15. Diagram showing possible cusp wedge traversals in high B_y cases: the Sun is towards the bottom of the figure marked by a 12, (a) The northern polar cap for duskward IMF (or southern polar cap for dawnward IMF), (b) The northern polar cap for dawnward IMF (or southern polar cap for duskward IMF). In each case, a satellite track represented by the gray arrow would see a V structure, while a satellite track, marked as black, would not. (Adapted from Crooker, 1988).

exit times of each passage through the boxes were compiled without regard to IMF direction.

Once the cusp crossing times had been compiled, each time was used to calculate a time-shift for IMF data taken by the IMP-8 satellite (when available). This time shift was subsequently used to calculate an average IMF for each pass, which was converted into one of 8 clock angle sectors in the GSM *y*-*z* plane. Once all of these data had been collected, the crossing times were used to create spectrogram images for each cusp crossing. The filenames were time tagged with the beginning time, and included codes for which hemisphere the spacecraft was in, as well as the IMF clock angle during the pass. These image files were then manually sorted by content. First, a list of "successful" cusp passes was compiled, success being defined as having a clear cusp signature in the ion and electron spectrogram data. Next, possibly relevant passes were noted for closer examination. A more detailed look was then taken of the candidate passes so that they could be correctly categorized. This process was repeated for all of the satellites examined, and the results compiled together.

3.2. Survey results

After examining over 3700 cusp passes from the Astrid-2 and four DMSP satellites, it became clear that these small-scale V's are not equally likely at all orientations of the IMF. Figure 16 is a histogram of occurrences vs. the eight IMF bins showing the combined data for all of the satellites in the study. The number of observed passes from each satellite has been weighted relative to the percentage of passes occurring during each of the eight IMF clock angles. This general morphology occurs, however, within each individual satellite data set both weighted and unweighted. This robust statistical trend clearly shows a preference for strong IMF B_y, with a lesser preference towards southward IMF. It is interesting to note that the data also show a strong preference for duskward over dawnward IMF, the occurrence of the duskward peak being 2.4 times the dawnward peak value. This is probably due to the available angles with which the various spacecraft passed through the cusp region. In the orbits used in the study, the angle between the satellite tracks and noon MLT is such that, in the North, a wedge pointing duskward (for duskward IMF) would be traversed more perpendicularly, while a dawnward pointing wedge would be crossed less perpendicularly, making the double signature visible less often (as in the black tracks of Figure 15). A similar argument holds for the southern hemisphere, keeping in mind that in the South the wedge moves in the direction opposite the IMF, rather than with it. A "V" signature is expected only if the spacecraft crosses both arms of the wedge. Given the traversal direction of the passes, this is much more likely in the South for dusk-pointing fields than for dawn-pointing fields.

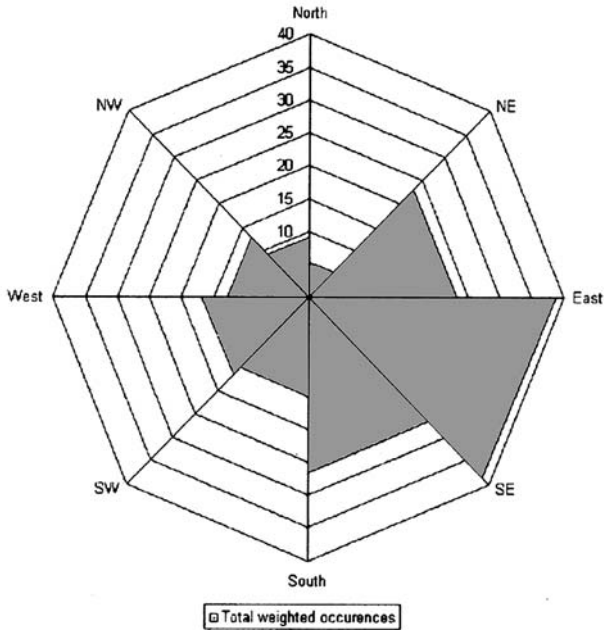

Figure 16. Histogram of weighted "V" Occurrences vs. IMF clock angle. A strong duskward and weaker dawnward peak can be seen, as expected from theoretical considerations.

Overall, some sort of cusp was seen in the particle data for about 40% of the passes studied. Of those, about 10% contained a V signature. This is a very reasonable percentage for a persistent feature with an average size of about 0.75° in Invariant Latitude and only 0.28 h of Magnetic Local Time (at the cut angles available in this study). The uneven sampling of the box by the satellites used in the study limits the conclusions that can be drawn about the cusp's overall movements within the box; clearly it moves around a great deal, and its shape and position are strongly influenced by the IMF at the magnetopause. The picture that emerges from this statistical survey is of a consistently present limited region within the cusp that is governed by the IMF direction and tends to stretch longitudinally with increasing B_y, making it more likely to be encountered by polar-orbiting satellites.

4. Discussion

We have presented cusp-related data from several different satellites, instruments and altitudes, representing various sensor types and technologies. The fact that the narrow "V" feature is consistent throughout all of the data sets indicates that it is not a characteristic of the instruments taking the data, but must be considered to be a real structure. Also, the fact that the

energetic particle and field instruments see a feature at the same time with a comparable scale-size also points to it being something physical. The feature is also persistent, as the statistical survey of Astrid-2 and DMSP data has shown.

Reiff et al. (1977) discuss convective dispersion, an injection model which they called for northward IMF – "diffusive injection"; it assumes a dependence on energy for the rate of diffusion from a central "injection field line." This results in an energy dispersion in which the highest energy particles are towards the edges of the cusp (since they can random walk farther from their injection point than the lower energy particles). Later works (Reiff et al., 1980; Burch et al., 1980; Woch and Lundin, 1992; Weiss et al., 1995) confirmed that these features are seen, usually during northward IMF conditions, and offered other explanations for these "large scale V's". Possible explanations such as tail reconnection, changes in the IMF B_z, and lobe reconnection have been offered. The features presented here, however, are of a scale size much smaller than the large V dispersion features studied by these authors, and appear to be very localized to the equatorward edge of the precipitating particle region. For this work, we have defined 300 km to be the break in scale size (at low altitudes) between the two types of features. It is clear that in the complex 3-D geometry of the cusp there are multiple ways to cut through in order to create a "V" in the ion spectrograms, so this distinction should be viewed simply as one more step towards fully parsing the features of the cusp into understandable components. It should also be noted that, while the large-scale V's have been found to occur predominantly during northward IMF conditions, the small V's have been shown here to have a minimum at that orientation. While some characteristics and possible causes of these two structures no doubt overlap, we believe that they are not equivalent.

The scale size, plasma characteristics, shape and location of this feature are all consistent with the Crooker model (1985, 1988) of the narrow wedge cusp presented in the Introduction. This feature should always be present, but its size and variable orientation naturally limit the extent to which it can be observed. A spacecraft trajectory is unlikely to cross the full potential difference across the V, so that only for relatively lucky crossings when the V structure is lying significantly across the trajectory would the feature be visible. This wedge cusp can be defined in terms of the magnetopause current layer, which contains the outermost layer of magnetic field lines of the magnetosphere. This very thin layer is the site of the interconnection between the Earth's magnetic field and the interplanetary magnetic field and produces other interesting processes, not all of which are understood. The low-altitude regions to which these outermost field lines map are the magnetic cusps (i.e., defined by field geometry rather than particle population), which we believe are associated with this small sub-region of the particle-defined cusp, called

the ''true cusp'' by Keith et al. (2001). Thus, this ''true cusp'' can represent a unique window into the large-scale workings of the magnetosphere and the magnetopause current layer. Newell and Meng (1991) noted a spatially distinct region of accelerated plasma at the equatorward edge of the cusp very similar to these observations, although with a less favorable geometry for seeing the structure clearly. They also argue against temporal variations as a cause, due to the fact that the accelerated region is always at the equatorward edge of the cusp.

The primary difference between this definition and that of the cusp proper is that the particles are expected to be more energetic, reflecting the populations accelerated through non-MHD processes in the magnetopause current layer and seen by *in situ* measurements (Gosling et al., 1986; Song et al., 1990) and simulations (Nakamura and Scholer, 2000). It is also possible for drifting energetic particles to become temporarily trapped in the outer cusp region from low latitudes (Sheldon et al., 1998; Delcourt and Sauvaud, 1999). Particles with pitch angles initially near 90° drift from the near-tail to the dayside magnetosphere (Figure 17, trajectories labeled 1, 2, and 3). Particles along 1, the innermost track, circulate in a well-behaved (ring-current) manner. The outermost third track reaches the equatorial dusk flank. Particles following the second (center) track, however, encounter a non-equatorial mirror force in the vicinity of the cusp where they are drawn to high latitudes and can become trapped temporarily in the local magnetic field minimum surrounding the cusp funnel. A portion of this population precipitates around the perimeter of the cusp funnel. Locally penetrating, unaccelerated magnetosheath plasma from the magnetopause boundary layer is also seen near the boundary (Lundin, 1988), and should propagate in the cusp proper to low-altitudes poleward (and occasionally equatorward) of the accelerated plasma population of the true cusp.

Mid-altitude data from Cluster, although preliminary, point to a temporally stable feature with a great deal of structure at the transition region between the turbulence-dominated exterior cusp region described by Savin et al. (1998) and the more stable, Crooker (1985, 1988)-like wedge cusp seen at lower altitudes. The correlation of the data between the four Cluster spacecraft is most easily explained by their varying altitudes, even though the spacecraft were relatively close. The data from the lower satellites looked more similar to those expected for the Crooker cusp, while the higher ones contained characteristics found in the Savin et al. (1998) exterior cusp. This observation must be investigated further to help establish the existence of such a transition region at mid altitudes.

A survey of over 3700 cusp passes taken from five different satellite platforms confirms the strong preference of IMF direction expected from the Crooker (1988) model of the cusp. The movements of the cusp and the angle through which it is traversed by the spacecraft all influence the shape of the

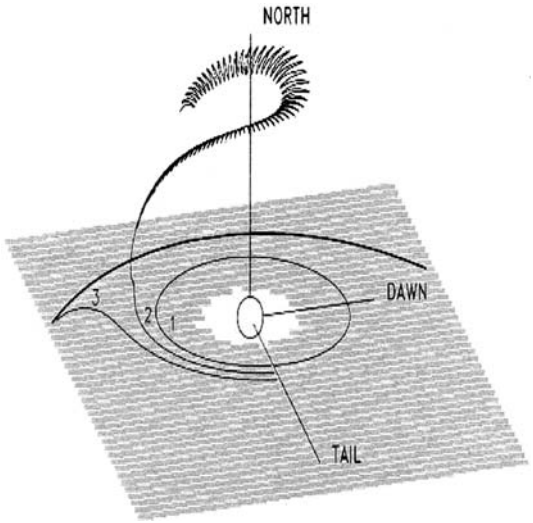

Figure 17. Equatorial ring current particles drift from the plasma sheet to the dayside magnetopause region and are deflected into a cusp-orbiting trajectory. From here they may be lost along the edges of the cusp to low altitudes. (From Delcourt and Sauvaud, 1999).

spectrogram that is seen; however, the experimental evidence points to a cusp that swings from side to side with the IMF, and is very limited in size. The evidence from the survey is, therefore, supportive of the existence of a true cusp region in the form of a wedge that responds to the Interplanetary Magnetic Field by rotating and extending in Magnetic Local Time.

5. Conclusions

An important, yet small-scale feature has been presented here; it is consistent with the wedge cusp of Crooker (1988), and with the turbulent exterior cusp. The location and energization of these features fits our expectation of a mapping of the magnetopause current layer, which has been previously reported in Keith et al. (2001). It is hoped that, as more high-resolution, low and mid altitude data become available, new information about the cusp and the associated particle entry processes may be derived.

Although more work is certainly needed in order to fully understand this unique feature, it is clear from these initial investigations that a window to the larger workings of the magnetosphere exists at low-altitudes, perhaps even more so than previously thought (Newell and Meng, 1995). The data studied indicate a unique feature in the cusp, distinct from the remaining cusp precipitation, which we believe to be the low altitude mapping of the magnetopause current layer, i.e., the true cusp. As more detailed work is

conducted, it is hoped that this model may be integrated to a further degree with the overall mainstream picture of the cusp and its dynamics.

The data presented here are consistent with a measurable low altitude image of the magnetopause current layer. These field lines are those on which ions are accelerated above magnetosheath energies and which form the classical magnetic cusp (i.e., *not* a plasma cusp). The mapping topology at low and mid altitudes appears to "swing" with B_y as expected from the Crooker (1988) model and has an enhanced electric field, as predicted. The wave data in the ELF/ULF region are consistent with the observations of a turbulent, noisy magnetopause. Energetic particles seen at the edges of the V feature are consistent with drifting particles that see a non-equatorial mirror force (Sheldon et al., 1998; Delcourt and Sauvaud, 1999) near the magnetopause and drift up into the magnetic cusp where they circulate and can be lost. The transition region from the turbulent exterior cusp has been sampled by the set of Cluster spacecraft, indicating a continuum between the morphologies seen at high altitudes and those seen at low altitudes.

Future work will focus on understanding in greater detail the connections between the IMF, magnetopause current layer and the cusp. This includes the addition of new data, especially from the Cluster mission, which has already begun to revolutionize our understanding of these regions. Recent DMSP data can hopefully be used along with Cluster to study concurrent mid and low altitude passages. It is hoped that this work may lead to a consensus on the methods of charged particle entry in the magnetopause and on the relationship of the magnetopause current layer to the cusp.

Acknowledgements

This work is supported by NASA grant NAG510863. We would like to acknowledge Nelson Maynard for the use of DE-2 VEFI data, Donald Gurnett for DE-1 PWI data, and the NSSDC OMNIWeb and participating investigators for solar wind and IMF data.

Appendix A

The earliest observations presented are from the High Altitude Plasma Instrument (HAPI) and the Low Altitude Plasma Instrument (LAPI) on the DE-1 and −2 satellites. HAPI uses five parabolic electrostatic analyzers at fixed viewing angles of $\pm 45°$, $\pm 12°$, and 0 (relative to the spin axis (Burch et al., 1981). LAPI consists of 15 parabolic electrostatic analyzers covering

180° for ions and electrons from 5 eV to 32 keV and two Geiger–Mueller (G–M) counters that measure >35 keV electrons at 0° and 90° pitch angles relative to the magnetic field. The spectrometers take one 32-step spectrum each second from each sensor (Winningham et al., 1981).

The U.S. Air Force's SSJ/4 particle instruments on the DMSP satellites comprise the highest volume of data studied, thanks to multiple satellite platforms covering many years of operations. SSJ/4 is a set of four cylindrical electrostatic analyzers, two sensors each (high and low energies) for both electrons and ions. Together they cover an energy range from 30 eV to 30 keV, completing a spectrum once per second. The DMSP satellites are non-spinning, and the SSJ/4 detectors are mounted such that they are always pointed radially outwards from the Earth. Near the northern (southern) polar cusp, this zenith direction will be close to the (anti)parallel magnetic field direction. Further information about the DMSP program and the SSJ/4 instruments can be found in Hardy et al. (1984).

Data have also been presented from the MEDUSA-1 and −2 instruments flown aboard the Swedish Astrid-2 and Munin spacecraft, respectively. The Miniaturized Electrostatic DUal-top-hat Spherical Analyzer (MEDUSA) was first flown aboard the Swedish Astrid-2 microsatellite (Marklund, 2001). The instrument is composed of two spherical top-hat analyzers placed top-to-top with a common 360° field of view. Each detector is divided into 16 azimuthal sectors of 22.5°, with an elevation acceptance of about 5°. They have an energy per charge range of about 1 eV to 20 keV for electrons and positive ions. A second, almost identical unit, MEDUSA-2, was flown aboard the Munin nanosatellite. The Munin spacecraft was locked to the Earth's magnetic field such that the 16 MEDUSA-2 input sectors looked in constant pitch angle directions. MEDUSA-1 has a sample rate for ions of 8 sweeps per second, and 16 sweeps per second for electrons. The sample rates for MEDUSA-2 are one quarter those of MEDUSA-1 due to telemetry limitations. More information on the MEDUSA instruments can be found in Keith (1999) and Norberg et al. (2001). Astrid-2 also had a fields experiment named Electric and Magnetic field Measurements for Astrid-2 (EMMA). EMMA (Blomberg, 2001) measures two spin-plane components of the electric field and all three components of the magnetic field.

The HEPS instrument on the UARS satellite studying high-energy electrons and ions (from 30 keV to 5 MeV and 150 MeV, respectively) consists of four electron/proton detectors, two electron detectors, and two Low Energy Proton (LEP) detectors. The MEPS spectrometer is made up of eight parabolic plate electrostatic analyzers and looks at electrons and ions in the 1 eV to 32 keV range. Each detector is situated on the spacecraft so as to have a different look direction angle with respect to the spacecraft (Winningham et al., 1993).

Recent Cluster data complete the list. Particle detection for this mission is spread over several experiments on each spacecraft. We are primarily interested in electron data from the Plasma Electron and Current Experiment (PEACE) and ion data from the Cluster Ion Spectrometry (CIS) experiment. PEACE consists of two sensors with hemispherical electrostatic analyzers, each with a 180° field of view radially outwards and perpendicular to the spin plane. Together, the sensors cover an energy range from 0.6 eV up to 26 keV over twelve polar sectors (Johnstone et al., 1997). CIS also consists of two sensors, one with ion mass resolution and the other without. Both have spherical electrostatic energy analyzers, the mass resolving instrument CODIF covers four ion species from 20 eV to 40 keV/charge, while the non-mass-resolving unit HIA has an energy range from 5 eV to 32 keV. Each instrument is divided into two 180° fields of view tangential to the spin axis with different sensitivities. The high sensitivity sides face spinward and cover all polar angles, while the low sensitivity sides face anti-spinward (Rème et al., 1997). The STAFF Spectrum Analyzer computes the electric and magnetic waves fluctuations at 27 frequencies distributed logarithmically in the frequency range from 8 Hz to 4 kHz (Cornilleau-Wehrlin et al., 1997). Detailed information on all of the instruments for the Cluster mission can be found in Escoubet et al., (1997).

References

Aparicio, B., Thelin, B., and Lundin, R.: 1991, 'The Polar Cusp From a Particle Point of View: A Statistical Study Based on Viking Data', *J. Geophys. Res.* **96**, 14023–14031.

Bonnell, J., Elphic, R. C., Palfrey, S., Strangeway, R. J., Peterson, W. K., Klumpar, D., Carlson, C. W., Ergun, R. E., and McFadden, J. P.: 1999, 'Observations of polar cap arcs on FAST', *J. Geophys. Res.* **104**, 12669–12681.

Burch, J. L., Reiff, P. H., Heelis, R. A., Spiro, R. W., and Fields, S. A.: 1980, "Cusp region particle precipitation and ion convection for northward interplanetary magnetic field", *Geophys. Res. Lett.* **7**, 393–396.

Burch, J. L., Winningham, J. D., Eaker, N., Blevins, V. A., and Hoffman, R. A.: 1981, 'The High Altitude Plasma Instrument (HAPI)', *Space Sci. Inst.* **5**, 455–463.

Chapman, S., and Ferraro, V.C.A.: 1931, 'A new theory of magnetic storms', *Terr. Magn. Atmos. Electr.* **36**, 171–186.

Cornilleau-Wehrlin, N., Chauveau, P., Louis, S., Meyer, A., Nappa, J. M., Perraut, S., Rezeau, L., Robert, P., Roux, A., Villedary, C.de, Conchy, Y.de, Friel, L., Harvey, C. C., Hubert, D., Lacombe, C., Manning, R., Wouters, F., Lefeuvre, F., Parrot, M., Pincon, J. L., Poirier, B., Kofman, W., and Louarn, P.: 1997, 'The CLUSTER Spatio-Temporal Analysis of Field Fluctuations (STAFF) Experiment', *Space Sci. Rev.* **79**, 107–136.

Crooker, N. U.: 1985, 'A Split Separator Line Merging Model of the Dayside Magnetopause', *J. Geophys. Res.* **90**, 12104–12110.

Crooker, N. U.: 1988, 'Mapping the Merging Potential From the Magnetopause to the Ionosphere Through the Dayside Cusp', *J. Geophys. Res.* **93**, 7338–7344.

Delcourt, D. C., and Sauvaud, J.-A.: 1999, 'Populating of the Cusp and Boundary Layers by Energetic (Hundreds of keV) Equatorial Particles'', *J. Geophys. Res.* **104**, 22635–22648.

Dubinin, E., Skalsky, A., Song, P., Savin, S., Kozyra, J., Moore, T. E., Russell, C. T., Chandler, M. O., Fedorov, A., Avanov, L., Sauvaud, J.-A., and Friedel, R. H.W.: 2002, 'Polar-Interball coordinated observations of plasma and magnetic field characteristics in the regions of the northern and southern distant cusps', *J. Geophys. Res.* **107**, SMP 2-1.

Escoubet, C. P., Russell, C. T., and Schmidt, R. (eds.): 1997, '*The Cluster and Phoenix Missions*', Kluwer Academic Publishers.

Gosling, J. T., Thomsen, M. F., Bame, S. J., and Russell, C. T.: 1986, 'Accelerated Plasma Flows at the Near-Tail Magnetopause', *J. Geophys. Res.* **91**, 3029.

Gurnett, D. A., Anderson, R. R., Tsurutani, B. T., Smith, E. J., Paschmann, G., Haerendel, G., Bame, S. J., and Russell, C. T.: 1979, 'Plasma Wave Turbulence at the Magnetopause: Observations From ISEE 1 and 2', *J. Geophys. Res.* **84**, 7043–7058.

Hardy, D. A., Schmitt, L. K., Gussenhoven, M. S., Marshall, F. J., Yeh, H. C., Schumaker, T. L., Huber, A., and Pantazis, J.: 1984, *'Precipitating electron and ion detectors (SSJ/4) for the block 5D/flight 6-10 DMSP satellites: Calibration and data presentation', Rep. AFGL-TR-84-0314.*, Air Force Geophys. Lab, Hanscom Air Force Base, Mass.

Heikkila, W. J., and Winningham, J. D.: 1971, 'Penetration of Magnetosheath Plasma to Low Altitudes Through the Dayside Magnetospheric Cusps', *J. Geophys. Res.* **76**, 883–891.

Heikkila, W. J.: 1972. '*The Morphology of Auroral Particle Precipitation*.' Space Res. XII, Akademie-Verlag, Berlin, pp. 1343.

Johnstone, A. D., Alsop, C., Burge, S., Carter, P. J., Coates, A. J., Coker, A. J., Fazakerley, A. N., Grande, M., Gowen, R. A., Gurgiolo, C., Hancock, B. K., Narheim, B., Preece, A., Sheather, P. H., Winningham, J. D., and Woodliffe, R. D.: 1997, 'PEACE: A Plasma Electron and Current Experiment', *Space Sci. Rev.* **79**, 351–398.

Keith, W. R.: 1999, 'Development of an Ion/Electron Plasma Spectrometer,' Master of Science Thesis, Rice University, Houston, Texas.

Keith, W. R., Winningham, J. D., and Norberg, O.: 2001, 'A New, Unique Signature of the True Cusp', *Ann. Geophys.* **19**, 611–619.

Lundin, R.: 1998, 'On the Magnetospheric Boundary Layer and Solar Wind Energy Transfer into the Magnetosphere', *Space Sci. Rev.* **48**, 263–320.

Marklund, G. T., Blomberg, L. G., and Persson, S.: 2001, 'Astrid-2, an Advanced Microsatellite for Auroral Research', *Ann. Geophys.* **19**, 589–592.

Nakamura, M., and Scholer, M.: 2000, 'Structure of the magnetopause reconnection layer and of flux transfer events: Ion kinetic effects', *J. Geophys. Res.* **105**, 23179–23191.

Newell, P. T., and Meng, C.-I.: 1988, 'The Cusp and Cleft/Boundary Layer: Low Altitude Identification and Statistical Local Time Variation', *J. Geophys. Res.* **93**, 14549–14556.

Newell, P. T., and Meng, C.-I.: 1991, 'Ion Acceleration at the Equatorward Edge of the Cusp: Low altitude Observations of Patchy Merging', *Geophys. Res. Lett.* **18**, 1829–1832.

Newell, P. T., and Meng, C.-I.: 1995, 'Magnetopause Dynamics as Inferred from Plasma Observations on Low-Altitude Satellites', *AGU Geophys. Monogr.* **90**, 407–416.

Norberg, O., Winningham, J. D., Lauche, H., Keith, W., Puccio, W., Olsen, J., Lundin, K., and Scherrer, J.: 2001, 'The MEDUSA electron- and ion spectrometer and the PIA photometers on Astrid-2', *Ann. Geophys.* **19**, 593–600.

Paschmann, G., Haerendel, G., Sckopke, N., Rosenbauer, H., and Hedgecock, P. C.: 1976, 'Plasma and Magnetic Field Characteristics of the Distant Polar Cusp near Local Noon: The Entry Layer', *J. Geophys. Res.* **81**, 2883–2889.

Reiff, P. H.: 1979, Low Altitude Signatures of the Boundary Layers. In: Battrick, B, Proceedings of Magnetospheric Boundary Layers, Alpbach, 11–15 June 1979, ESA SP-148, Noordwijk, Netherlands, pp. 167–173.

Reiff, P. H., Hill, T. W., and Burch, J. L.: 1977, 'Solar Wind Plasma Injection at the Dayside Magnetospheric Cusp', *J. Geophys. Res.* **82**, 479–491.

Reiff, P. H., Burch, J. L., and Spiro, R. W.: 1980, 'Cusp Proton Signatures and the Interplanetary Magnetic Field', *J. Geophys. Res.* **85**, 5997–6005.

Rème, H., Bosqued, J. M., Sauvaud, J. A., Cros, A., Dandouras, J., Aoustin, C., Bouyssou, J., Camus, Th., Cuvilo, J., Martz, C., Médale, J. L., Perrier, H., Romefort, D., Rouzaud, J., D'Uston, C., Möbius, E., Crocker, K., Granoff, M., Kistler, L. M., Popecki, M., Hovestadt, D., Klecker, B., Paschmann, G., Scholer, M., Carlson, C. W., Curtis, D. W., Lin, R. P., McFadden, J. P., Formisano, V., Amata, E., Bavassano-Cattaneo, M. B., Baldetti, P., Belluci, G., Bruno, R., Chionchio, G., Di Lellis, A., Shelley, E. G., Ghielmetti, A. G., Lennartsson, W., Korth, A., Rosenbauer, H., Lundin, R., Olsen, S., Parks, G. K., McCarthy, M., and Balsiger, H.: 1997, 'The cluster ion spectrometry (CIS) Experiment', *Space Sci. Rev.* **79**, 303–350.

Savin, S. P., Borodkova, N. L., Budnik, E.Yu., Fedorov, A. O., S. I., Klimov, Nozdrachev, M. N., Morozova, I. E., Nikolaeva, N. S., Petrukovich, A. A., Pissarenko, N. F., Prokhorenko, V. I., Romanov, S. A., Skalsky, A. A., Yermolaev, Yu.I., Zastenker, G. N., Zelenyi, L. M., Triska, P., Amata, E., Blecki, J., Juchniewicz, J., Buechner, J., Ciobanu, M., Grard, R., Haerendel, G., Korepanov, V. E., Lundin, R., Sandahl, I., Eklund, U., Nemecek, Z., Safrankova, J., Sauvaud, J. A., Rustenbah, J., and Rauch, J. L.: 1998, 'Interball Tail Probe Measurements in Outer Cusp and Boundary Layers', *AGU Geophys. Monogr.* **104**, 25–44.

Sheldon, R. B., Spence, H. E., Sullivan, J. D., Fritz, T. A., and Chen, J.: 1998, 'The discovery of trapped energetic electrons in the outer cusp', *Geophys. Res. Lett.* **25**, 1825–1828.

Song, P., Elphic, R. C., Russell, C. T., Gosling, J. T., and Cattell, C. A.: 1990, 'Structure and Properties of the Subsolar Magnetopause for Northward IMF: ISEE Observations', *J. Geophys. Res.* **95**, 6375–6387.

Stasiewicz, K.: 1991, 'Polar Cusp Topology and Position as a Function of Interplanetary Magnetic Field and Magnetic Activity: Comparison of a Model With Viking and Other Observations', *J. Geophys. Res.* **96**, 15789–15800.

Weiss, L. A., Reiff, P. H., Webber, E. J., Carlson, H. C., Lockwood, M., and Peterson, W. K.: 1995, 'Flow-Aligned Jets in the Magnetospheric Cusp: Results From the Geospace Environment Modeling Pilot program', *J. Geophys. Res.* **100**, 7649–7659.

Winningham, J. D., Burch, J. L., Eaker, N., Blevins, V. A., and Hoffman, R. A.: 1981, 'The Low Altitude Plasma Instrument (LAPI)', *Space Sci. Inst.* **5**, 465–475.

Winningham, J. D., Sharber, J. R., Frahm, R. A., Burch, J. L., Eaker, N., Black, R. K., Blevins, V. A., Andrews, J. P., Rudski, J., Sablik, M. J., Chenette, L. D., Datlowe, D. W., Gaines, E. E., Imhof, W. I., Nightingale, R. W., Reagan, J. B., Robinson, R. M., Schumaker, T. L., Shelley, E. G., Vondrak, R. R., Voss, H. D., Bythrow, P. F., Anderson, B. J., Potemra, T. A., Zanetti, L. J., Holland, D. B., Rees, M. H., Lummerzheim, D., Reid, G. C., Roble, R. G., Clauer, C. R., and Banks, P. M.: 1993, 'The UARS Particle Environment Monitor', *J. Geophys. Res.* **98**, 10649–10666.

Woch, J., and Lundin, R.: 1992, 'Magnetosheath Plasma Precipitation in the Polar Cusp and Its Control by the Interplanetary Magnetic Field', *J. Geophys. Res.* **97**, 1421–1430.